



Enhanced mechanical properties of high pressure solidified CoCrFeNiMo_{0.3} high entropy alloy via nano-precipitated phase

Duo Dong ^{a,c}, Wentao Jiang ^b, Xiaohong Wang ^c, Tengfei Ma ^c, Dongdong Zhu ^{a,c,*}, Ye Wang ^{b,**}, Juntao Huo ^d

^a School of Materials Science and Engineering, Taizhou University, Taizhou, 318000, China

^b School of Materials Science and Chemical Engineering, Harbin University of Science and Technology, Harbin, 150040, China

^c Key Laboratory of Air-Driven Equipment Technology of Zhejiang Province, Quzhou University, Quzhou, 324000, China

^d Chinese Academy of Sciences Ningbo Institute of Materials Technology and Engineering, Ningbo, 315201, China



ARTICLE INFO

Keywords:

High entropy alloy
High pressure solidification
Microstructure
Nano-indentation

ABSTRACT

CoCrFeNiMo_{0.3} high entropy alloy was prepared by vacuum arc melting. The effects of different solidification pressures on the microstructure and mechanical properties of CoCrFeNiMo_{0.3} high entropy alloy were investigated. All ambient pressure (0.1 MPa) Mo_{0.3}, 4 GPa Mo_{0.3} and 7 GPa Mo_{0.3} alloys exhibit two kinds of structures. The FCC structure is the solid solution matrix, and the precipitated phase enrich in Cr and Mo (σ phase) is distributed in the grain boundary of the matrix phase. With the increase of the test pressure, the size of the precipitated phase gradually decreases and the volume fraction increases obviously, and tends to form nano-scale particles. Meanwhile, the precipitated phase gradually diffused into the matrix due to the increase of the pressure. The results of nanoindentation tests show that the hardness of the alloy increases significantly with the increase of solidification pressure, especially that of 7 GPa Mo_{0.3} alloy, which is about 2 times that of 0.1 MPa Mo_{0.3} alloy. The strengthening mechanism of CoCrFeNiMo_{0.3} high entropy alloy with increased pressure is mainly nano-precipitated strengthening. This present findings not only pave the way for designing the structure and property regulation of high pressure solidified HEAs but also promote the application orientation of various property combinations. It provides the theoretical basis for its application and is expected to be used as structural materials in various fields.

1. Introduction

Traditional alloys system usually consist of one or two main elements, and the content of other elements is much lower than that of the main elements. The addition of other elements is usually used to improve the properties of the alloy. High entropy alloy (HEA) is defined as containing n main elements (usually $n \geq 5$), each of which has a concentration between 5 % and 35 %. Its appearance breaks the empirical design concept of traditional alloys and opens up a broad space for alloy design [1–3]. The higher mixing entropy makes the high entropy alloy more inclined to form a simple solid solution phase (FCC structure or BCC structure), and exhibits various interesting and unusual properties [4–8]. Researchers have summarized its unique properties as high entropy effect in thermodynamics, lattice distortion effect in structure, hysteretic diffusion effect in dynamics and cocktail effect in

properties [9,10]. These unique properties make the high entropy alloy possess many excellent properties such as high strength, high hardness, high temperature stability, high wear resistance and corrosion resistance [11,12]. Therefore, high entropy alloy has always been the research hotspot in the field of materials since it was proposed.

Among many FCC high entropy alloys, CoCrFeNi system high entropy alloys have become an important research branch of high entropy alloys system due to their excellent corrosion resistance, ductility and structural stability [13]. However, the CoCrFeNi system high entropy alloys have a low mechanical strength, which cannot meet the production requirements of high strength and high hardness parts. Relevant studies have indicated that the addition of Al, Mn, Mo and other elements to the CoCrFeNi system high entropy alloys can form an ordered strengthening phase, resulting in precipitation strengthening and improving the mechanical properties of the alloy such as strength and

* Corresponding author. School of Materials Science and Engineering, Taizhou University, Taizhou, 318000, China.

** Corresponding author.

E-mail addresses: zhudd8@163.com (D. Zhu), ohenry1980@163.com (Y. Wang).

hardness [4,6,14–17]. For example, CoCrFeMnNi high entropy alloy, known as “Cantor alloy”, with the temperature dropping from 293 K to 77 K, its yield strength increases significantly, and reaches 759 MPa, and its elongation even exceeds 70 %. Such excellent low temperature property is due to the continuous mechanical hardening caused by the formation of nano-twinning from adjacent lattice atoms during the deformation process [4]. However, the strength of the CoCrFeMnNi alloy in structural applications is relatively weak [12]. Adding Mo element to CoCrFeNi alloy can precipitate brittle intermetallic compounds and significantly improve the properties of the CoCrFeNi alloy [13,15]. For both solid solution and precipitated strengthening, the size of Mo element is moderate. Although its plasticity at room temperature is not satisfactory, the combination of physical and mechanical properties gives it excellent comprehensive properties such as high hardness and oxidation resistance. In addition, Liu and Shun et al. [14,18] reported the mechanical properties of (FeCoCrNi)-Mo system alloys. The study showed that the addition of Mo promoted the solid solution strengthening and precipitation strengthening, which greatly improved the strength of FeCoCrNi alloy. Whether in BCC-based HEAs or FCC-based HEAs, the presence of intermetallic compound phases (like sigma, B2 type, silicide phase) may optimize the microstructure of the alloy, thereby enhancing its various properties [19–22]. For example, the precipitation of σ and μ intermetallic compounds significantly increases the hardness of CrMnFeCoMo alloy (9.3 GPa) [20]. Therefore, the reasonable introduction of intermetallic compounds may have unexpected gains in the study of the microstructure and properties of alloys.

A large number of studies have shown that the properties of substances can be improved by the regulation of composition or preparation temperature. One way to improve the properties of a substance is to change the external pressure. High pressure technology has been widely used in various disciplines, and led to the emergence of many interdisciplinary disciplines. Under high pressure, the distance between atoms decreases, and the crystal structure and electronic structure of the alloy are changed, thus forming a microstructure different from that under ambient pressure, which is of great research value [23–25]. In addition, the pressure can not only reduce the defects in the alloy, but also change the nucleation and growth mode of the alloy, so as to refine the grain, improve the mechanical and physical properties of the alloy, and induce drastic changes in the distribution, composition, morphology and size of the second phase [26,27]. At present, the researches on high pressure solidification mainly focus on Al series alloys. Although the types of alloys studied are different, their variation rules are very similar. After high pressure solidification, the microstructure of the alloy is refined to a great extent, and the phase nucleation is promoted, which leads to the change of phase morphology. In addition, the diffusion of atoms is effectively inhibited at high pressure. Therefore, the solid solubility of the solute in the alloy prepared by high pressure solidification technology is greatly improved. As a high-strength, high toughness, and high wear resistant alloy material, high-entropy alloys have broad application prospects in fields such as aerospace, high-speed rail, and energy [28,29]. Compared with traditional alloys, high-entropy alloys have better processing and formability, and can manufacture more complex and precise components and products. Therefore, combining high-pressure solidification technology with high-entropy alloys can provide more reliable and efficient technical means for the manufacturing and application of high-entropy alloys, and also provide more innovative ideas and application scenarios for the development of related fields.

Although high pressure solidification provides a new method to control and optimize the microstructure of the alloy, there are few studies on the microstructure and properties of high-entropy alloy under different pressure solidification so far. Therefore, in the present work, CoCrFeNiMo_{0.3} high-entropy alloy was prepared by vacuum arc melting, and high pressure solidified CoCrFeNiMo_{0.3} high-entropy alloy was obtained by changing the solidification pressure, and the evolution of its

microstructure and mechanical properties were studied. This study is expected to provide important experimental significance and guidance for the development of high pressure solidification technology to prepare new high entropy alloys.

2. Experimental procedures

Co, Cr, Fe, Ni and Mo particles with at least 99.9 wt% purity were selected as raw materials and mixed according to the molar ratio of 1: 1: 1: 1: 0.3. All raw materials were removed before weighing, ultrasonic cleaning with 95 % industrial alcohol to remove impurities on the surface of the raw materials and blow dry. The CoCrFeNiMo_{0.3} high entropy alloy was obtained by using DHL-500 II non-consumable vacuum arc melting furnace under a high purity argon atmosphere. Prior to melting, one of the water-cooled copper crucible places pure sponge Ti to initiate the arc and absorb the residual oxygen in the furnace. The alloys ingots must be melted at least 5 times to ensure that all metal elements are completely melted and the alloy composition is homogeneous.

The CoCrFeNiMo_{0.3} alloy button ingots were cut into cylinders (Φ 3 mm \times 3.7 mm) using wire electrical discharge machining (WEDM). After grinding and polishing, the high-pressure solidification test is carried out using the German Max-Vogggenreiter high-temperature high-pressure press with the model of LPR1000-400/50. The assembly block must be prepared before the high-pressure synthesize. During the assembly of the high-pressure sample, graphite tube is used as the heating furnace, zirconia is used as the insulation layer, and pyrophyllite is used as the packaging material and pressure transmission medium. Then, put the assembled sample into the center of the cube which composed of 8 WC hammers. Finally, put them all into the chamber of the equipment. During high pressure synthesis, first, increase the pressure to the target value (4 GPa and 7 GPa). Then, raise the temperature to 1800K over the course of 1 h, hold it for 15 min. Finally, cool it to room temperature and release the pressure. For the convenience of discussion, the CoCrFeNiMo_{0.3} alloys obtained by different pressure were defined as ambient pressure (0.1 MPa) Mo_{0.3}, 4 GPa Mo_{0.3} and 7 GPa Mo_{0.3} alloys respectively in this paper.

The phase and crystal structure of 0.1 MPa Mo_{0.3}, 4 GPa Mo_{0.3} and 7 GPa Mo_{0.3} alloys were identified with X-ray diffractometer by using a Germany D8 Advance X-ray diffractometer with Cu- $\kappa\alpha$ radiation. The scanning range of diffraction angle (2θ) is 20°–100°, with a scanning rate of 4°/min, the tube voltage of 40 V, and the tube current of 40 mA. The samples were carefully polished to observe the microstructure of the alloys. The microstructure of CoCrFeNiMo_{0.3} high entropy alloy after high pressure solidification was observed by Hitachi SU8010 scanning electron microscope (SEM). SU8010 scanning electron microscope was equipped with backscattered electron (BSE) detector and energy dispersive spectroscopy (EDS) detector to obtain the phase composition and the distribution of elements in the microstructure of 0.1 MPa Mo_{0.3}, 4 GPa Mo_{0.3} and 7 GPa Mo_{0.3} alloys before and after electrochemical polishing. Electrochemistry is used to polish the alloy, and the electrolytic solution required is HClO₄: C₂H₅OH = 1: 9. The test conditions are 20 V, 0.3–0.4 A, and polished for 12–15 s. Then the ultrasonic cleaning was carried out with 95 % industrial alcohol for 8 min to remove impurities. The volume fractions of different phases in the alloy were measured by Image J software. The nano-structures of 0.1 MPa Mo_{0.3} and 7 GPa Mo_{0.3} alloys were observed and analyzed by TECNAI G2 F30 field emission transmission electron microscope (TEM) under a voltage of 200 kV. Before the samples for TEM testing were mechanically ground to <60 μ m, then ion thinned by using a GATAN 691 precision ion

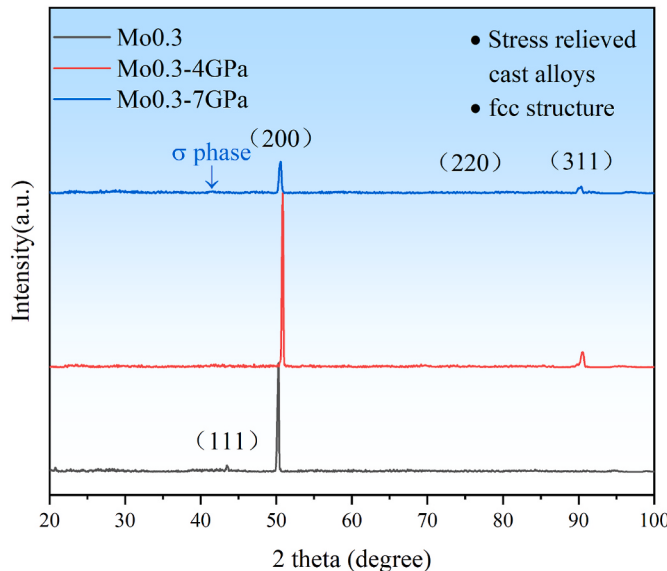
Table 1

Atomic percentage and mass percentage of CoCrFeNiMo_{0.3} high entropy alloy.

Element	Fe	Co	Cr	Ni	Mo
at.%	23.26	23.26	23.26	23.26	6.96
wt.%	21.97	23.19	20.46	23.09	11.29

Table 2Calculated parameters of ΔH_{mix} , ΔS_{mix} , T_m , Ω , δ , and VEC.

Alloy	$-\Delta H_{mix}$, kJ/mol	ΔS_{mix} , J/(mol K)	T_m , K	Ω	δ , %	VEC
Mo0.3	4.15	12.83	1943	6.01	4.41	8.09

**Fig. 1.** XRD patterns of the 0.1 MPa Mo_{0.3}, 4 GPa Mo_{0.3} and 7 GPa Mo_{0.3} high entropy alloys.

polishing system. The nanohardness test was performed by an automated, high-throughput TI-950 nanoindentation instrument developed by HYSITRON. The parameters used in the nanoindentation experiment are as follows: the maximum displacement at room temperature is 1000 nm, the loading and unloading rates are both 60 mN/min, and the holding time after reaching the maximum displacement is 30 s. 30 times nanoindentation tests were performed on each sample.

3. Results and discussion

3.1. Phase prediction

The atomic percentage and mass percentage composition of CoCrFeNiMo_{0.3} high entropy alloy are listed in Table 1, respectively. Generally, Mo element can be added to CoCrFeNi medium entropy alloy to form precipitated phase [18,30]. For CoCrFeNiMo_{0.3} high entropy alloy, the equivalent chromium content (ECC) equation can be used to evaluate whether the alloy has precipitated phase formation [31], and the calculation formula is as follows:

$$\begin{aligned} ECC = & Cr\% + 0.31\%Mn + 1.76\%Mo + 0.97\%W + 2.02\%V + 1.58\%Si + 2.44\%Ti \\ & 1.7\%Nb + 1.22\%Ta - 0.266\%Ni - 0.177\%Co \end{aligned} \quad (1)$$

where, if the equivalent Cr content (ECC) is greater than 17–18 wt%, precipitated phase is easy to be generated in the alloy [31]. By substituting the mass percentage of each element listed in Table 1 into Eq. (1), the ECC value is 31.0 wt%, which is easy to form precipitated phase.

In addition, several important criteria based on thermodynamic and geometric effects can also be used to predict the phase formation of the CoCrFeNiMo_{0.3} high entropy alloy. The relevant parameters are calculated by the following formula [32–37]:

$$\Delta H_{mix} = \sum_{i=1, i \neq j}^n 4c_i c_j \Delta H_{ij}^{mix} \quad (2)$$

$$\Delta S_{mix} = -R \sum_{i=1}^n c_i \ln c_i \quad (3)$$

$$T_m = \sum_{i=1}^n c_i (T_m)_i \quad (4)$$

$$\Omega = \frac{T_m \Delta S_{mix}}{|\Delta H_{mix}|} \quad (5)$$

$$\delta = \sqrt{\sum_{i=1}^n c_i \left(1 - r_i / \left(\sum_{i=1}^n c_i r_i \right) \right)^2} \quad (6)$$

$$VEC = \sum_{i=1}^n c_i (VEC)_i \quad (7)$$

Where c_i and c_j represent the atomic percentage of elements i and j in the alloy system, respectively, $R = 8.314 \text{ J}/(\text{mol}\cdot\text{K})$ is the gas constant, c_i and c_j are the atomic percentages, T_m is the theoretical melting temperature of the alloy system, Ω is used to predict the formation of solid solution phases in alloys system, δ is used to describe the comprehensive effect of the difference of atomic-size in CoCrFeNiMo_{0.3} high entropy alloy, r_i is the atomic radius, and VEC is the mixture valence electron concentration of the alloy. The calculation results of each parameter are listed in Table 2. Relevant studies have shown that when $\Omega > 1.1$, $\delta < 6.6 \%$, ΔH_{mix} is in the range of $-20\text{--}5 \text{ kJ/mol}$, the alloy is more inclined to form solid solution [34], and the larger the Ω value, the smaller the δ value, the more obvious the tendency to form solid solution. The mixing enthalpy of the CoCrFeNiMo_{0.3} high entropy alloy is -4.15 kJ/mol , and the values of Ω and δ are 6.01 and 4.41 %, respectively, which conform to the formation criterion of solid solution phase. Valence electron concentration (VEC) can be used to quantitatively predict the formation of BCC or FCC phases in high entropy alloys [35]. It is generally believed that a simple FCC phase will be formed when $VEC \geq 8.0$. When $6.87 \leq VEC \leq 8.0$, BCC phase and FCC phase exist simultaneously. When $VEC \leq 6.87$, a simple BCC phase will be formed. The calculated valence electron concentration of CoCrFeNiMo_{0.3} high entropy alloy is 8.09, which belongs to FCC structure. Based on the above prediction of phase composition, CoCrFeNiMo_{0.3} high entropy alloy has a two-phase structure, that is, it is composed of FCC solid solution phase and Cr-containing intermetallic compound precipitated phase.

3.2. Phase identification

The XRD results of the 0.1 MPa Mo_{0.3}, 4 GPa Mo_{0.3} and 7 GPa Mo_{0.3}

high entropy alloys are shown in Fig. 1. The alloy appears to exhibit only a single FCC structure under the solidification pressure of 0.1 MPa and 4 GPa, due to its high mixing entropy effect, which effectively reduces the Gibbs free energy in the mixing process, thus promoting the formation of face-centered cubic solid solution during the solidification process. Therefore, it is reasonable to believe that the FCC structure constitutes the matrix of the alloy, while in the 7 GPa Mo_{0.3} alloy, the σ phase of the tetragonal structure seems to be formed near $20\text{--}40^\circ$. Further analysis of the crystal structure of each alloy was conducted using Jade 6.5

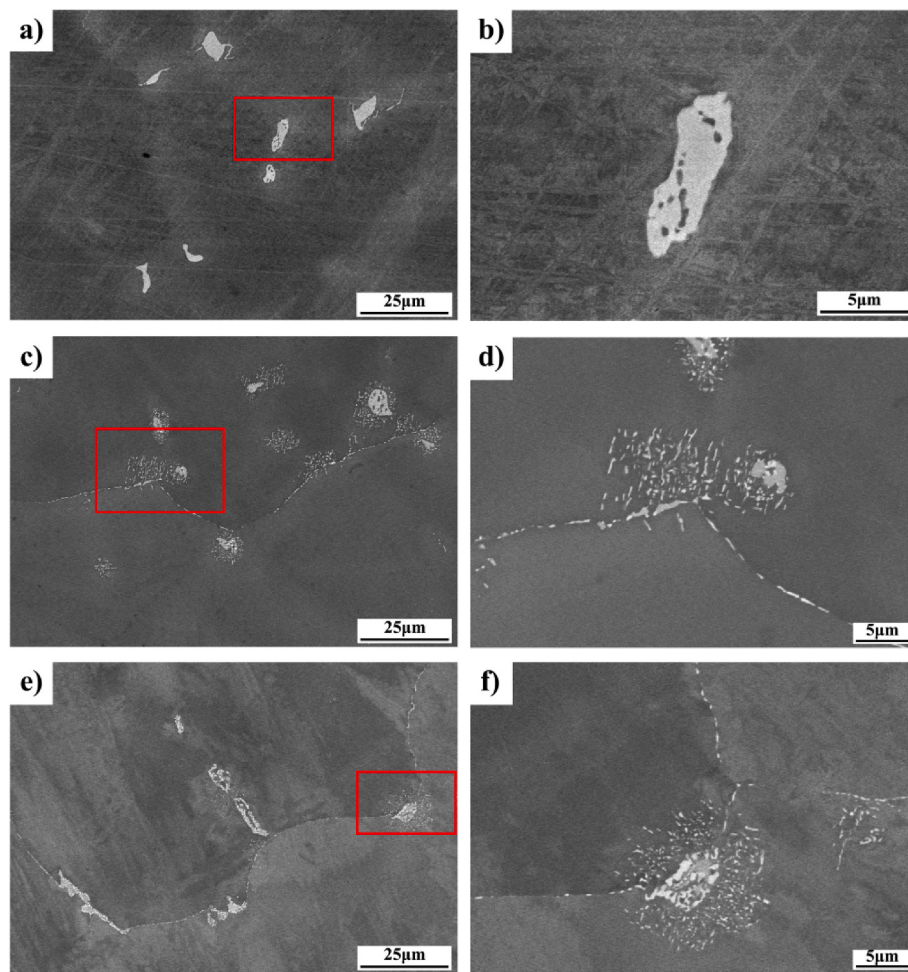


Fig. 2. SEM-BSE images of the CoCrFeNiMo_{0.3} high entropy alloy: (a) 0.1 MPa Mo_{0.3} alloy, (b) Enlarged BSE image of 0.1 MPa Mo_{0.3} alloy, (c) 4 GPa Mo_{0.3} alloy, (d) Enlarged BSE image of 4 GPa Mo_{0.3} alloy, (e) 7 GPa Mo_{0.3} alloy, (f) Enlarged BSE image of 7 GPa Mo_{0.3} alloy.

software, the lattice parameters of 0.1 MPa Mo_{0.3}, 4 GPa Mo_{0.3} and 7 GPa Mo_{0.3} alloys were 3.632, 3.577 and 3.604 Å, respectively. The increase in pressure leads to a decrease in the lattice parameter of the alloy, causing diffraction peaks to shift towards higher angles and a gradual decrease in the intensity of the (110) diffraction peaks of the alloy (the diffraction angles of the (110) diffraction peaks of 0.1 MPa Mo_{0.3}, 4 GPa Mo_{0.3} and 7 GPa Mo_{0.3} alloys are 44.08°, 44.13°, and 44.61°, respectively, which are slightly higher than the diffraction angles of sigma phase). Note that the lattice parameter of the 4 GPa Mo_{0.3} alloy is the smallest and exhibits an abnormally high strength texture in the (200) direction, which may be due to the use of vacuum melting to prepare the sample, while this preferred orientation can disappear in powder materials [15].

3.3. Microstructure characterization

Fig. 2 displays the scanning electron microscope (SEM) images of the CoCrFeNiMo_{0.3} alloy solidified at different high pressures under back-scattered electrons. All 0.1 MPa Mo_{0.3}, 4 GPa Mo_{0.3} and 7 GPa Mo_{0.3} alloys show two distinct contrast regions, combined with XRD results, the dark gray area is FCC solid solution matrix, and the light gray area is σ phase. The measurement results of Image J software show that the volume fractions of the FCC matrix phase in 0.1 MPa Mo_{0.3}, 4 GPa Mo_{0.3}, and 7 GPa Mo_{0.3} alloys are 98.62 %, 98.65 %, and 98.68 %, respectively, and the volume fractions of σ phase are 1.38 %, 1.35 % and 1.32 %, respectively. The change in pressure did not have a significant impact on the phase composition and volume fraction of the alloy, while

the change in morphology was more pronounced. The σ phase in 0.1 MPa Mo_{0.3} alloy is rod-like and disperses in FCC solid solution matrix, with its size between 5 and 10 μm, and no obvious grain boundaries were observed in the 0.1 MPa Mo_{0.3} alloy. As the testing pressure increases, some can still be seen σ phase precipitates in the matrix and clusters together. In addition, a large number of rod-like σ phases with a size of about 1 μm are precipitated at the grain boundaries (as shown in Fig. 2(d)), making the alloy grain boundaries gradually become obvious. This also indicates that solidification under high pressure conditions makes it easier for the alloy to precipitate a second phase and distribute it at grain boundaries, while pressure can cause significant refinement of the second phase. When the test pressure increases to 7 GPa, as shown in Fig. 2e and f, the volume fraction of σ phase in the crystal decreased significantly, while the σ phase precipitated at the grain boundary showed more spherical morphology, with a size far less than 1 μm. This also indicates that the increase in pressure will also promote σ Spheroidization. Smaller particle sizes help to resist deformation under external stress and enhance the mechanical properties of the alloy [20].

According to the above SEM observation results, σ phase is mostly concentrated at the grain boundaries of the alloy matrix. Therefore, to more directly observe the influence of different solidification pressures on the microstructure of CoCrFeNiMo_{0.3} alloy, electrochemical polishing was carried out on the surface of the alloy. The microstructure of the treated alloy under scanning electron microscope is displayed in Fig. 3. The different regions in the 0.1 MPa Mo_{0.3}, 4 GPa Mo_{0.3} and 7 GPa Mo_{0.3} alloys are marked as A and B, respectively. Structure A is dendrite region (DR) and structure B is interdendrite (ID). Both 0.1 MPa Mo_{0.3} and 4 GPa

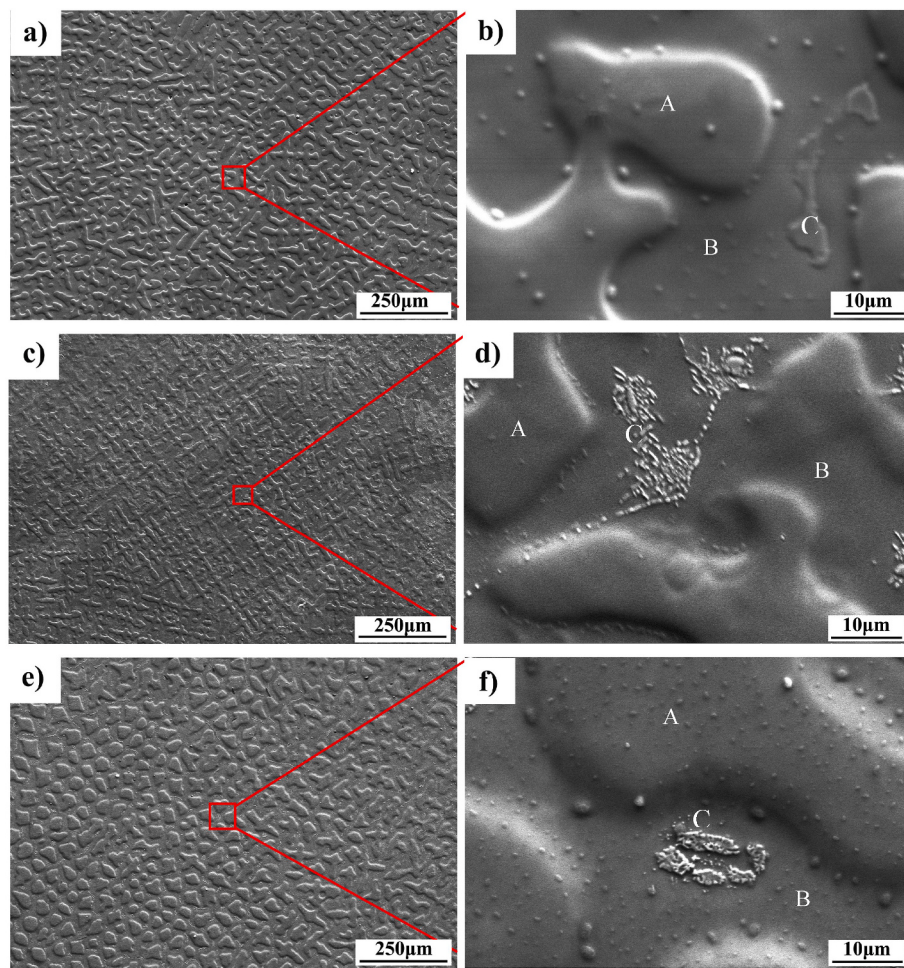


Fig. 3. SEM - SE images of the CoCrFeNiMo_{0.3} high entropy alloy after electropolishing: (a) 0.1 MPa Mo_{0.3} alloy, (b) Enlarged BSE image of 0.1 MPa Mo_{0.3} alloy, (c) 4 GPa Mo_{0.3} alloy, (d) Enlarged BSE image of 4 GPa Mo_{0.3} alloy, (e) 7 GPa Mo_{0.3} alloy, (f) Enlarged BSE image of 7 GPa Mo_{0.3} alloy.

Table 3

Nominal and EDS point analysis results of the various region in 0.1 MPa Mo_{0.3}, 4 GPa Mo_{0.3} and 7 GPa Mo_{0.3} high entropy alloys.

Alloy	Phase	Chemical composition (at.%)				
		Fe	Co	Cr	Ni	Mo
Nominal composition		23.26	23.26	23.26	23.26	6.96
0.1 MPa Mo _{0.3}	DR, A (FCC)	24.98	26.14	21.69	24.17	3.01
	ID, B (FCC)	22.53	24.19	24.23	23.01	6.04
	ID, C (σ)	20.21	21.44	26.63	19.39	12.33
4 GPa Mo _{0.3}	DR, A (FCC)	25.04	25.09	22.24	24.54	3.09
	ID, B (FCC)	23.42	24.11	23.60	23.64	5.23
	ID, C (σ)	22.03	22.95	25.62	20.22	9.19
7 GPa Mo _{0.3}	DR, A (FCC)	24.71	25.38	21.88	24.91	3.12
	ID, B (FCC)	22.91	23.77	24.26	23.12	5.43
	ID, C (σ)	18.78	19.23	31.33	14.53	16.13

Mo_{0.3} alloys exhibit typical dendrite structures, and the primary dendrites of 0.1 MPa Mo_{0.3} alloys are relatively continuous. Different from the microstructure before electrochemical polishing, it can be observed from the enlarged microstructure image of 0.1 MPa Mo_{0.3} alloy (Fig. 3(b)) that there are many granular σ phases with a size of about 1 μm in the ID region. With the increase of solidification pressure, it can be observed that the dendrites of 4 GPa Mo_{0.3} alloy are obviously refined, and more granular σ phases are precipitated in the ID region. However, when the pressure increased to 7 GPa, no obvious primary dendrite structure can be observed in the microstructure of 7 GPa Mo_{0.3} alloy, and the grains in the DR region tend to grow equiaxial. This may be due to

the high pressure that causes Mo atom to diffuse to ID region and then combine with Cr element. As a result, Mo, which is an element with high melting point, cannot preferably form a primary dendrite arm coating during solidification, thus forming the morphology shown in Fig. 3(e). In addition, different from 0.1 MPa Mo_{0.3} and 4 GPa Mo_{0.3} alloys, more and finer granular σ phases appear in the matrix of 7 GPa Mo_{0.3} alloy. Table 3 shows the nominal chemical composition of CoCrFeNiMo_{0.3} alloy and EDS chemical composition analysis results of ID region, DR Region and σ phase in 0.1 MPa Mo_{0.3}, 4 GPa Mo_{0.3} and 7 GPa Mo_{0.3} alloys. Combined with the data in Table 3 and Fig. 3, the difference between regions A and B mainly lies in the difference of Mo content. The Mo content in ID region is significantly higher than that in DR region. In addition, with the increase of solidification pressure, the Mo content in the DR region increases somewhat, while the Mo content in the ID region increases significantly. Similarly, the Cr element in the ID region also increases significantly. Combined with the XRD results, both DR and ID regions are the same FCC phases, and there is a σ phase (structure C) enrich in Cr and Mo in ID region.

Fig. 4 provides the EDS map scanning results of the 0.1 MPa Mo_{0.3}, 4 GPa Mo_{0.3} and 7 GPa Mo_{0.3} high entropy alloys after electrochemical polishing. With the increase of solidification pressure, the distribution of Mo element in the interdendritics gradually becomes obvious. The results also indicate that high pressure makes the σ phase of CoCrFeNiMo_{0.3} high entropy alloy more likely to diffuse to the matrix and precipitate during the solidification process, and this tendency has a direct effect on the increase of pressure.

To further determine the nano-scale structure of the matrix phase

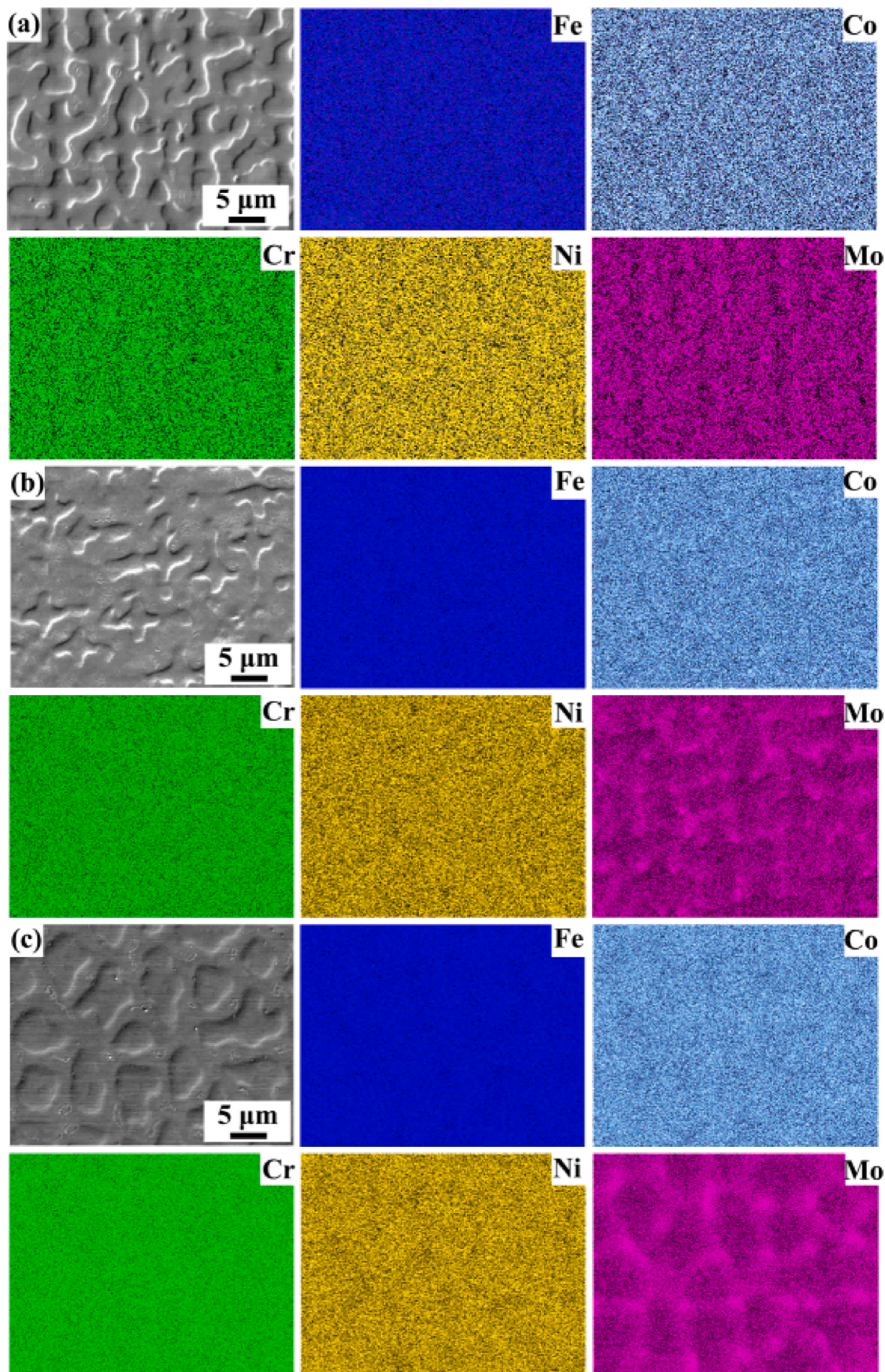


Fig. 4. Energy dispersive spectrometer (EDS) map scanning images of the FeCoCrNiMo_{0.3} high entropy alloy after electropolishing: (a) 0.1 MPa Mo_{0.3} alloy, (b) 4 GPa Mo_{0.3} alloy, (c) 7 GPa Mo_{0.3} alloy.

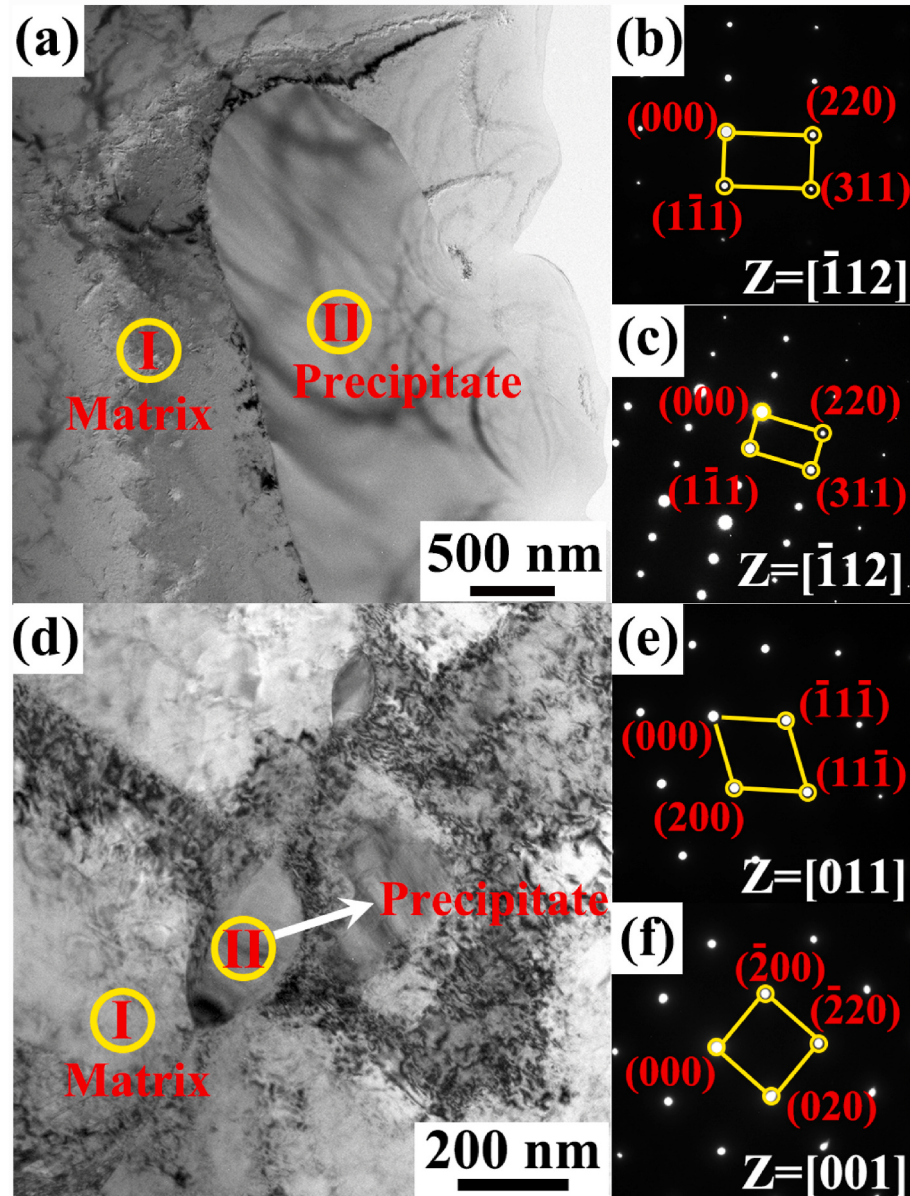


Fig. 5. TEM images of the 0.1 MPa $\text{Mo}_{0.3}$ and 7 GPa $\text{Mo}_{0.3}$ high entropy alloys: (a) Bright field image of the 0.1 MPa $\text{Mo}_{0.3}$ alloy, (b) SAED pattern of the circled region I in (a), (c) SAED pattern of the circled region II in (a), (d) Bright field image of the 7 GPa $\text{Mo}_{0.3}$ alloy, (e) SAED pattern of the circled region I in (d), (f) SAED pattern of the circled region II in (d).

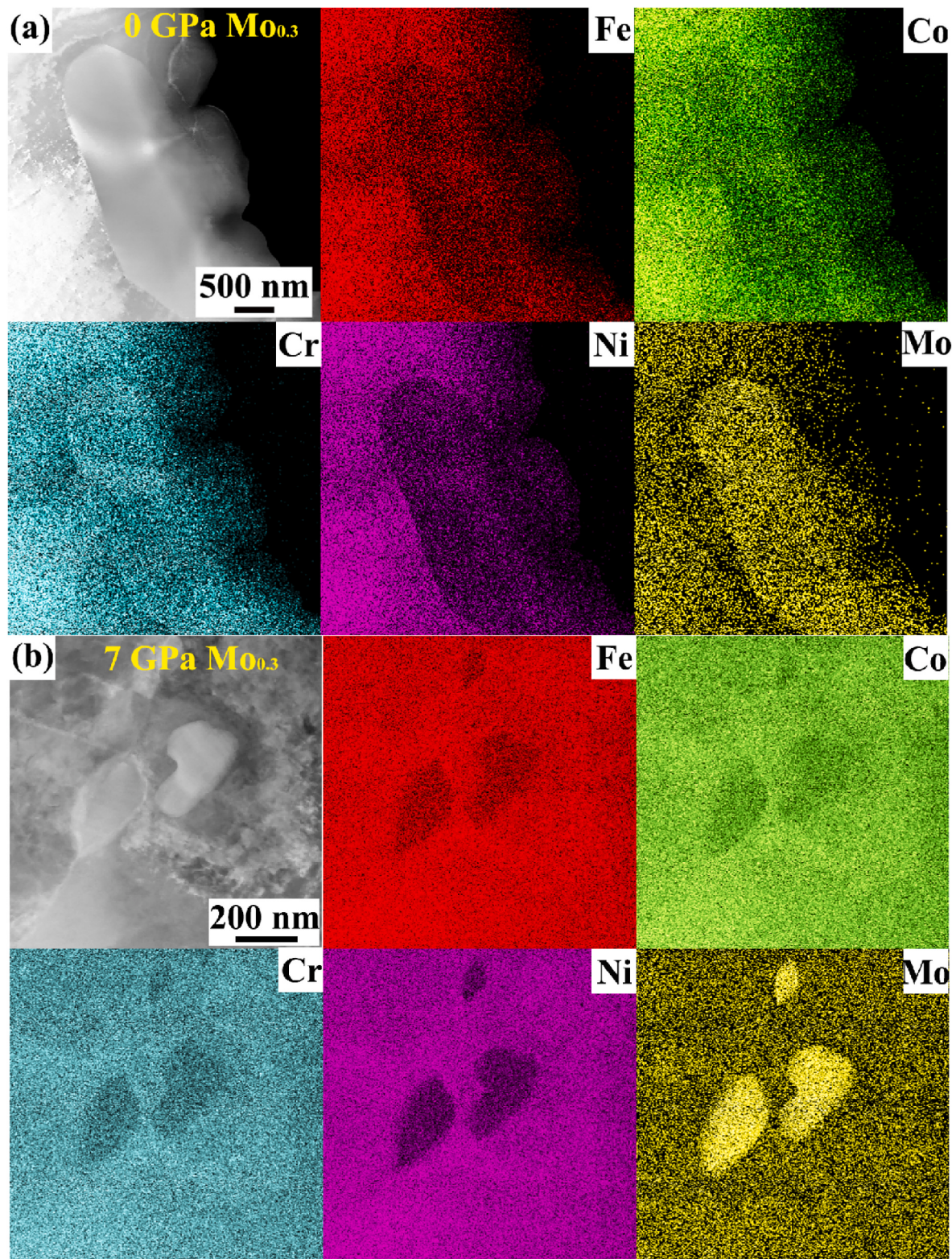


Fig. 6. TEM images of the 0.1 MPa Mo_{0.3} and 7 GPa Mo_{0.3} high entropy alloys: (a) HAADF-STEM micrograph of the 0.1 MPa Mo_{0.3} high entropy alloy and EDS map scanning showing the distribution of elements, (b) HAADF-STEM micrograph of the 7 GPa Mo_{0.3} high entropy alloy and EDS map scanning showing the distribution of elements.

Table 4

Nominal and EDS point analysis results of the various region in 0.1 MPa Mo_{0.3} and 7 GPa Mo_{0.3} high entropy alloys.

Alloy	Phase	Chemical composition (at.%)				
		Fe	Co	Cr	Ni	Mo
Nominal composition 0.1 MPa Mo _{0.3}	FCC phase	23.26	23.26	23.26	23.26	6.96
	σ phase	22.10	23.40	24.15	23.86	6.19
7 GPa Mo _{0.3}	FCC phase	17.96	21.25	30.43	14.61	16.75
	σ phase	22.75	23.52	24.85	22.60	6.29
		17.34	20.91	22.35	11.24	28.16

and precipitated phase, 0.1 MPa Mo_{0.3} alloy and 7 GPa Mo_{0.3} alloy were observed by transmission electron microscopy (TEM) and the diffraction pattern was calibrated. The bright field transmission electron microscopy images of 0.1 MPa Mo_{0.3} and 7 GPa Mo_{0.3} alloys are revealed in Fig. 5(a–c). The results also demonstrate that the size of precipitated phase decreases obviously with the increase of pressure. The matrix phase and precipitated phase regions in Fig. 5(a–c) are selected for electron diffraction. The selected area electron diffraction (SAED) further determines that the matrix and precipitated phase of 0.1 MPa Mo_{0.3} alloy and 7 GPa Mo_{0.3} alloy are σ phase with tetragonal structure and FCC structure, respectively, as shown in Fig. 5(b, c) and (e, f). The diffraction patterns of the selected area I and II of 0.1 MPa Mo_{0.3} alloy

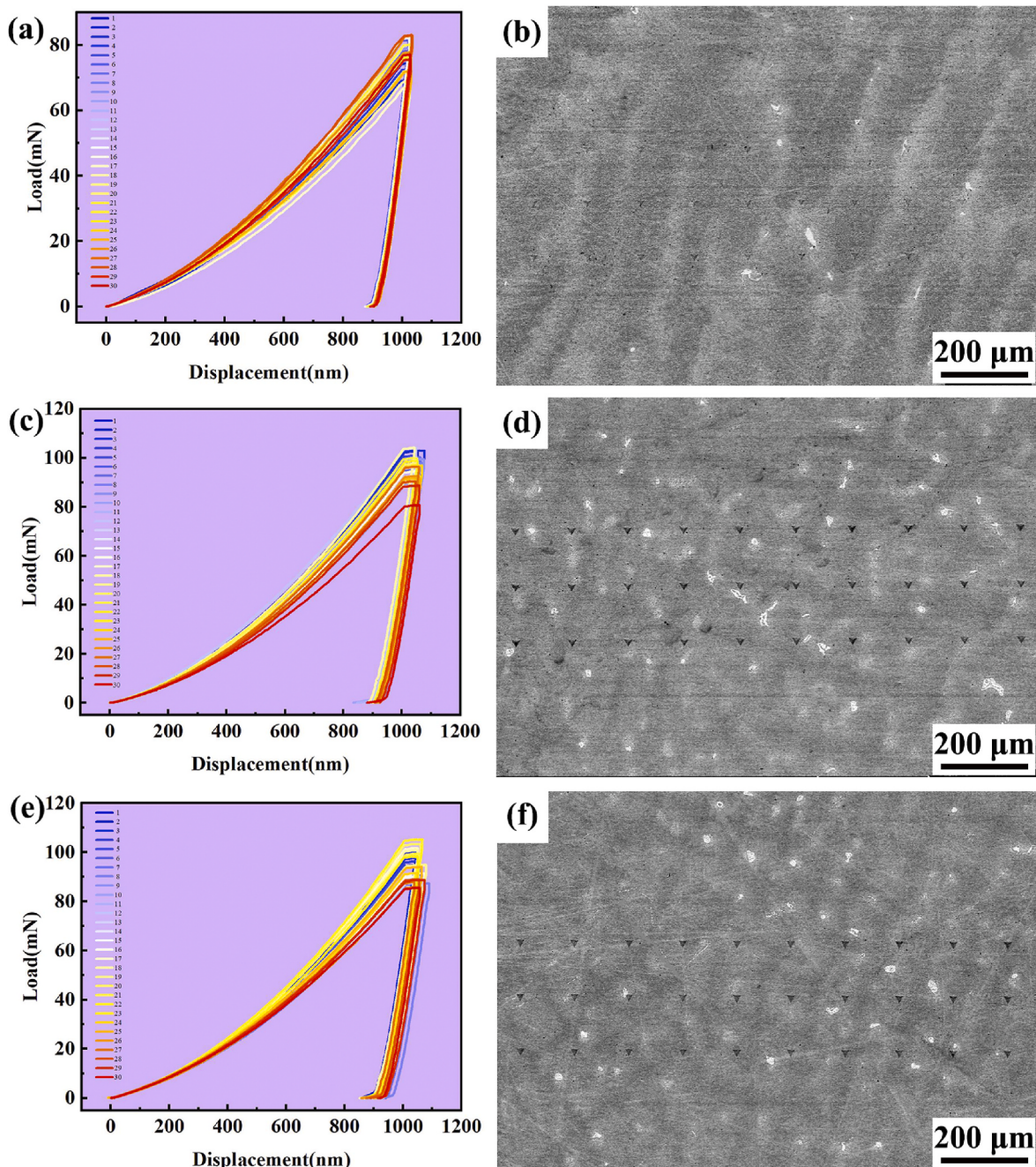


Fig. 7. Representative load-displacement curves of the FeCoCrNiMo_{0.3} high entropy alloy, and the micro-morphologies of the area where the nano-indentation is tested.

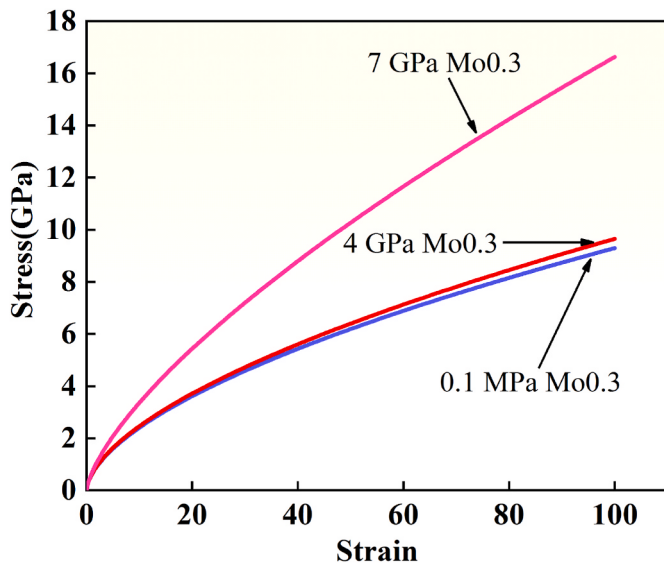


Fig. 8. The nanoindentation stress-strain curves of the high pressure solidified FeCoCrNiMo_{0.3} high entropy alloy based on parameters calculated from the proposed inverse method.

confirm that a FCC structure with [1 12] zone axis and a tetragonal structure with [1 12] zone axis, respectively, and the orientation relationship between the two phases is [1 12]_{FCC}//[1 12]_{FCC}. The diffraction patterns of the selected area I and II of 7 GPa Mo_{0.3} alloy confirm that a FCC structure with [011] zone axis and a tetragonal structure with [001] zone axis, respectively, and the orientation relationship between the two phases is [011]_{FCC}//[001]_σ.

Fig. 6 shows the high angle annular dark field scanning (HAADF-STEM) images and element distribution of the 0.1 MPa Mo_{0.3} and 7 GPa Mo_{0.3} alloys. Table 4 lists the EDS point scanning element distribution results of 0.1 MPa Mo_{0.3} and 7 GPa Mo_{0.3} alloys. Consistent with relevant references reports [18,30], the precipitated phase in 0.1 MPa Mo_{0.3} alloy is a σ phase enrich in Cr and Mo elements. However, an interesting phenomenon was found in the map scanning element distribution of 7 GPa Mo_{0.3} alloy. The contrast of Cr element in the σ phase with a diameter of ~300 nm is darker than that of the matrix, while only the contrast of Mo element is brighter. This may be due to the small atomic radius of Cr element (0.129 nm). The pressure of 7 GPa makes Cr more inclined to dissolve into the matrix. Combined with the data in Table 4, it is obvious that the increase of solidification pressure significantly increases the content of Mo element in precipitated phase.

3.4. Mechanical properties

Typical load-displacement (*p-h*) curves and the SEM images obtained by the corresponding nano-indentation test at different areas of FeCoCrNiMo_{0.3} high entropy alloy are shown in Fig. 7. The results show that the solidification pressure can significantly affect the hardness of the FeCoCrNiMo_{0.3} alloy. As the depth increases to 1000 nm, the load of 0.1 MPa Mo_{0.3} alloy can reach ~70 mN. The solidification pressure increases the hardness of the alloy, and both the load of 4 and 7 GPa Mo_{0.3} alloys can reach ~100 mN.

The plastic behavior of most metallic materials can be approximated by a power law, and the elastic-plastic behavior of materials can be described as [38]:

$$\left\{ \begin{array}{ll} \sigma = E\varepsilon & \sigma \leq \sigma_y \\ \sigma = \sigma_y \left(1 + \frac{E}{\sigma_y} \varepsilon_p \right)^n & \sigma \geq \sigma_y \end{array} \right. \quad (8)$$

where, E is the elastic modulus, σ_y is the yield strength, n is the hardening exponent, and ε_p is the nonlinear part of the total strain ε_y , which is accumulated over the yield strain ε_y , and is defined as:

$$\varepsilon_p = \varepsilon - \varepsilon_y \quad (9)$$

With the assumed power law in Eq. (8), the values E , σ_y and n determine the overall stress-strain of the material. According to the above equation, nano-indentation stress-strain curves of the FeCoCrNiMo_{0.3} high entropy alloy solidified at different high pressures can be obtained as given in Fig. 8. When the test strain reaches 100 %, the stress of 0.1 MPa Mo_{0.3} alloy is 9.3 GPa, and that of 7 GPa Mo_{0.3} alloy is 16.6 GPa, which is about twice as high as that of 0.1 MPa Mo_{0.3} alloy.

To further reveal the reason why different pressure changes the mechanical properties of FeCoCrNiMo_{0.3} high entropy alloys, transmission electron microscopy images of 0.1 MPa Mo_{0.3} and 7 GPa Mo_{0.3} high entropy alloys are demonstrated in Fig. 9. In Fig. 9(a), it can be seen that 0.1 MPa Mo_{0.3} alloy has a certain density of dislocation entanglement, and the dislocation motion is dominated by plane slip. However, higher density and smaller scale dislocation entanglement can be seen in the 7 GPa Mo_{0.3} alloy, indicating that the increase of test pressure leads to the increase of dislocation density in the alloy, which may be one of the reasons for the mechanical property improvement. Fig. 9(c and d) illustrates the high-resolution transmission electron microscope (HRTEM) images of 0.1 MPa Mo_{0.3} and 7 GPa Mo_{0.3} high entropy alloys, respectively. The random distribution of the elements in the alloy results in random contrast in the images [38–40]. Inverse Fast Fourier Transform (IFFT) is carried out on the selected area in Fig. 9(c and d), as shown in Fig. 9(e and f). No obvious lattice mismatch was found in 0.1 MPa Mo_{0.3} alloy, while a certain density of lattice mismatch was found in 7 GPa Mo_{0.3} alloy, which indicated that the increase of solidification pressure would change lattice constant and cause serious lattice distortion [39–41]. Therefore, the mechanical properties of the 7 GPa Mo_{0.3} high entropy alloy obtained by high pressure solidification are much higher than those of the as-cast 0.1 MPa Mo_{0.3} alloy.

4. Conclusions

In summary, this work uncovers that the mechanical properties of CoCrFeNiMo_{0.3} high entropy alloy can be improved by high pressure solidification technology. The CoCrFeNiMo_{0.3} high entropy alloy solidified under different pressures showcases two kinds of structures. The FCC structure enriched in Fe, Co and Ni is the solid solution matrix, and the precipitated phase rich in Cr and Mo (σ phase) is distributed in the grain boundary of the matrix. With the increase of solidification pressure, the size of precipitated phase decreases from 5 to 10 μm to less than 1 μm, which makes the precipitated phase gradually diffuse into the matrix and the distribution becomes dispersive. The increase of solidification pressure makes the nano-hardness of the alloy increase significantly. When the test strain reaches 100 %, the stress of 7 GPa Mo_{0.3} alloy reaches 16.6 GPa, which is about twice that of 0.1 MPa Mo_{0.3} alloy. The improvement of its property is mainly related to the refinement and precipitation of the σ phase caused by the increase of test pressure, which strengthening mechanism is nano-precipitated strengthening. This study reveals the feasibility of regulating the microstructure by high pressure solidification technology to improve the mechanical properties of HEAs, thus broadening the development of high entropy alloy and the application of high pressure solidification technology to new materials in the future.

CRediT authorship contribution statement

Duo Dong: Writing – review & editing, Writing – original draft. **Wentao Jiang:** Writing – original draft, Resources, Data curation. **Xiaohong Wang:** Software, Methodology. **Tengfei Ma:** Resources, Methodology, Investigation. **Dongdong Zhu:** Project administration,

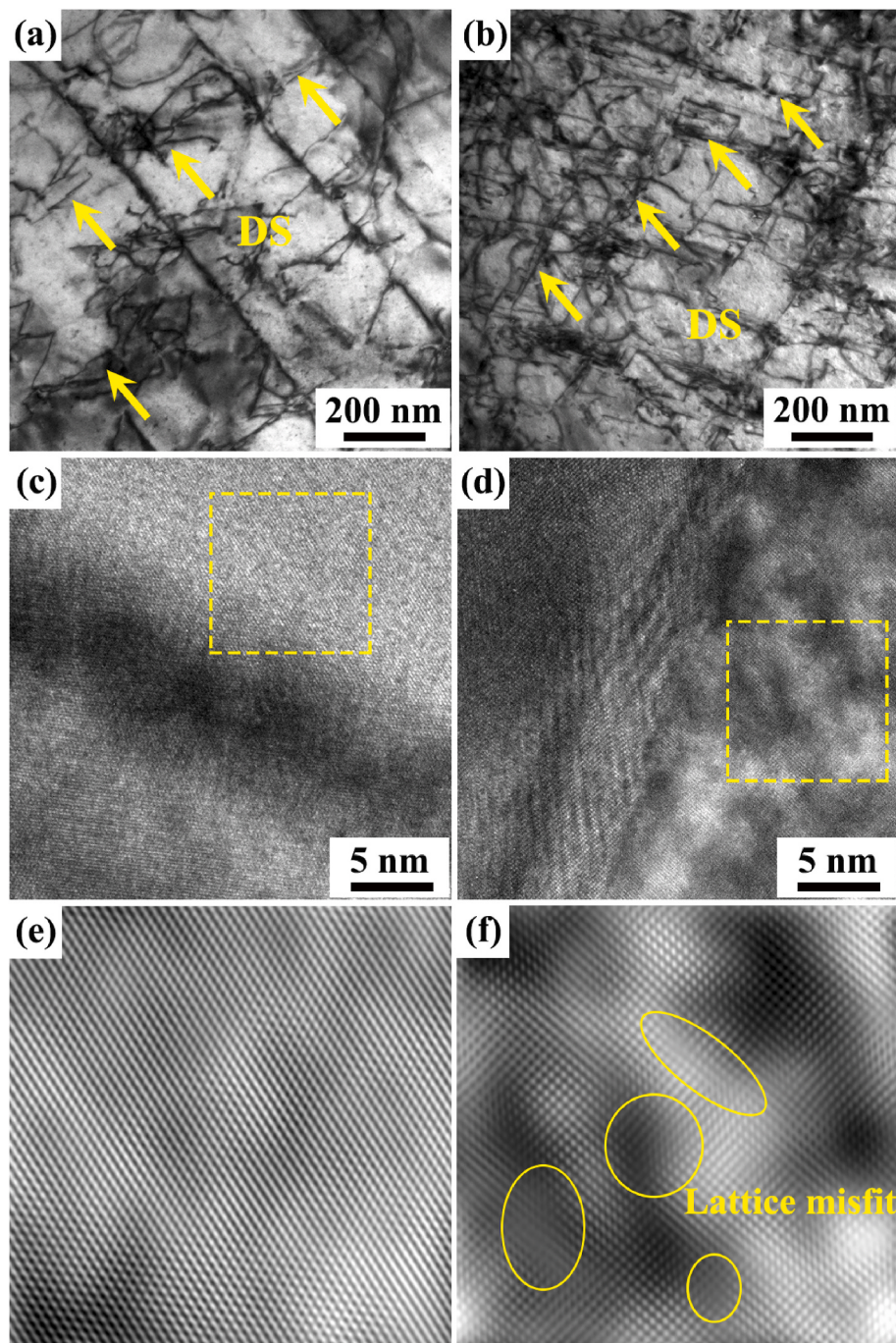


Fig. 9. (a) and (b) Bright field TEM image of the 0.1 MPa Mo_{0.3} alloy and 7 GPa Mo_{0.3} alloy showing the details of dislocations, (c) and (d) HRTEM images of the 0.1 MPa Mo_{0.3} alloy and 7 GPa Mo_{0.3} alloy, respectively, (e) and (f) Inversed FFT images of (c) and (d), respectively.

Funding acquisition. **Ye Wang:** Visualization, Supervision, Conceptualization. **Juntao Huo:** Supervision, Conceptualization.

Declaration of competing interest

The authors declare that they have no known competing financial interests or personal relationships that could have appeared to influence the work reported in this paper.

Data availability

Data will be made available on request.

Acknowledgment

This work was financially supported by the National Natural Science Foundation of China (No. 52171120, 52271106, 52071188), the Zhejiang Province Natural Science Foundation of China (LZY23E050001).

References

- [1] J.W. Yeh, S.K. Chen, S.J. Lin, J.Y. Gan, T.S. Chin, T.T. Shun, C.H. Tsau, S.Y. Chang, Nanostructured high-entropy alloys with multiple principal elements: novel alloy design concepts and outcomes, *Adv. Eng. Mater.* 6 (2004) 299–303, <https://doi.org/10.1002/adem.200300567>.

- [2] B. Cantor, I. Chang, P. Knight, A. Vincent, Microstructural development in equiaxial multicomponent alloys, *Mater. Sci. Eng. A* 375 (2004) 213–218, <https://doi.org/10.1016/j.msea.2003.10.257>.
- [3] Senkov, J.D. Miller, D.B. Miracle, C. Woodward, Accelerated exploration of multi-principal element alloys with solid solution phases, *Nat. Commun.* 6 (2015) 4, <https://doi.org/10.1038/ncomms7529>.
- [4] B. Gludovatz, A. Hohenwarter, D. Catoor, E.H. Chang, E.P. George, R.O. Ritchie, A fracture-resistant high-entropy alloy for cryogenic applications, *Science* 345 (2014) 1153–1158, <https://doi.org/10.1126/science.1254581>.
- [5] O.N. Senkov, S.V. Senkova, C.F. Woodward, Effect of aluminum on the microstructure and properties of two refractory high-entropy alloys, *Acta Mater.* 68 (2014) 214–228, <https://doi.org/10.1016/j.actamat.2014.01.029>.
- [6] Y. Tong, D. Chen, B. Han, J. Wang, R. Feng, T. Yang, C. Zhao, Y.L. Zhao, W. Guo, Y. Shimizu, C.T. Liu, P.K. Liaw, K. Inoue, Y. Nagai, A. Hu, J.J. Kai, Outstanding tensile properties of a precipitation-strengthened FeCoNiCrTi_{0.2} high-entropy alloy at room and cryogenic temperatures, *Acta Mater.* 165 (2019) 228–240, <https://doi.org/10.1016/j.actamat.2018.11.049>.
- [7] J. Li, Y. Chen, Q.F. He, X.D. Xu, H. Wang, C. Jiang, B. Liu, Q.H. Fang, Y. Liu, Y. Yang, P.K. Liaw, C.T. Liu, Heterogeneous lattice strain strengthening in severely distorted crystalline solids, *P. Natl. Acad. Sci. USA.* 119 (2022) 25, <https://doi.org/10.1073/pnas.2200607119>.
- [8] S.F. Liu, W. Kai, J.X. Hou, Y.L. Zhao, Q. Li, C.H. Yang, T. Yang, J.J. Kai, Oxidation behaviors and mechanical properties of L₁₂-strengthened high-entropy alloys at 700 °C, *Corrosion Sci.* 206 (2022) 110499, <https://doi.org/10.1016/j.corsci.2022.110499>.
- [9] Y. Zhang, T.T. Zuo, Z. Tang, M.C. Gao, K.A. Dahmen, P.K. Liaw, Z.P. Lu, Microstructures and properties of high-entropy alloys, *Prog. Mater. Sci.* 61 (2014) 1–93, <https://doi.org/10.1016/j.pmatsci.2013.10.001>.
- [10] Z.J. Wang, Y.H. Huang, Y. Yang, J.C. Wang, C.T. Liu, Atomic-size effect and solid solubility of multicomponent alloys, *Scripta Mater.* 94 (2015) 28–31, <https://doi.org/10.1016/j.scriptamat.2014.09.010>.
- [11] B. Gludovatz, A. Hohenwarter, D. Catoor, E.H. Chang, E.P. George, R.O. Ritchie, A fracture-resistant high-entropy alloy for cryogenic applications, *Science* 345 (2014) 1153, <https://doi.org/10.1126/science.1254581>.
- [12] W.T. Jiang, X.H. Wang, S.Y. Li, T.F. Ma, Y. Wang, D.D. Zhu, A lightweight Al_{0.8}Nb_{0.5}Ti₂V₂Zr_{0.5} refractory high entropy alloy with high specific yield strength, *Mater. Lett.* 328 (2022) 133144, <https://doi.org/10.1016/j.matlet.2022.133144>.
- [13] W.H. Liu, J.Y. He, H.L. Huang, H. Wang, Z.P. Lu, C.T. Liu, Effects of Nb additions on the microstructure and mechanical property of CoCrFeNi high-entropy alloys, *Intermetallics* 60 (2015) 1–8, <https://doi.org/10.1016/j.intermet.2015.01.004>.
- [14] B. Schuh, F. Mendez-Martin, B. Volker, E.P. George, H. Clemens, R. Pippan, A. Hohenwarter, Mechanical properties, microstructure and thermal stability of a nanocrystalline CoCrFeMnNi high-entropy alloy after severe plastic deformation, *Acta Mater.* 96 (2015) 258–268, <https://doi.org/10.1016/j.actamat.2015.06.025>.
- [15] W.H. Liu, Z.P. Lu, J.Y. He, J.H. Luan, Z.J. Wang, B. Liu, Y. Liu, M.W. Chen, C.T. Liu, Ductile CoCrFeNiMo_x high entropy alloys strengthened by hard intermetallic phases, *Acta Mater.* 116 (2016) 332–342, <https://doi.org/10.1016/j.actamat.2016.06.063>.
- [16] C.D. Zhao, J.S. Li, Y.D. Liu, X. Ma, Y.J. Jin, W.Y. Wang, H.C. Kou, J. Wang, Optimizing mechanical and magnetic properties of AlCoCrFeNi high-entropy alloy via FCC to BCC phase transformation, *J. Mater. Sci. Technol.* 86 (2021) 117–126, <https://doi.org/10.1016/j.jmst.2020.12.080>.
- [17] T.T. Shun, L.Y. Chang, M.H. Shiu, Microstructures and mechanical properties of multiprincipal component CoCrFeNiTi_x alloys, *Mater. Sci. Eng.* 566 (2012) 170–174, <https://doi.org/10.1016/j.msea.2012.06.075>.
- [18] T.T. Shun, L.Y. Chang, M.H. Shiu, Microstructure and mechanical properties of multiprincipal component CoCrFeNiMo_x alloys, *Mater. Char.* 70 (2012) 63–67, <https://doi.org/10.1016/j.matchar.2012.05.005>.
- [19] S. Kumar, A. Linda, Y. Shadangi, V. Jindal, Influence of micro-segregation on the microstructure, and microhardness of MoNbTaxTi(1-x)W refractory high entropy alloys: experimental and DFT approach, *Intermetallics* 164 (2024) 108080, <https://doi.org/10.1016/j.intermet.2023.108080>.
- [20] P. Pradhan, Y. Shadangi, V. Shivam, N.K. Mukhopadhyay, Powder metallurgical processing of CrMnFeCoMo high entropy alloy: phase evolution, microstructure, thermal stability and mechanical properties, *J. Alloys Compd.* 935 (2023) 168002, <https://doi.org/10.1016/j.jallcom.2022.168002>.
- [21] Y. Shadangi, K. Chattopadhyay, N.K. Mukhopadhyay, Powder metallurgical processing of Al matrix composite reinforced with AlSiCrMnFeNiCu high-entropy alloys: microstructure, thermal stability, and microhardness, *J. Mater. Res.* 38 (2023) 248–264, <https://doi.org/10.1557/s43578-022-00866-x>.
- [22] H. Jain, Y. Shadangi, D. Chakravarty, K. Chattopadhyay, A.K. Dubey, N. K. Mukhopadhyay, Low-density Fe₄₀Mn₁₉Ni₁₅Al₁₅Si₁₀C₁ high entropy steel processed by mechanical alloying and spark plasma sintering: phase evolution, microstructure and mechanical properties, *Mater. Sci. Eng. A* 869 (2023) 144776, <https://doi.org/10.1016/j.msea.2023.144776>.
- [23] J.S. Schilling, The use of high pressure in basic and materials science, *J. Phys. Chem. Solid.* 59 (1998) 4 553–568.
- [24] S.M. Sharma, S.K. Sikka, Pressure induced amorphization of materials, *Prog. Mater. Sci.* 40 (1996) 1–77, [https://doi.org/10.1016/0079-6425\(95\)00006-2](https://doi.org/10.1016/0079-6425(95)00006-2).
- [25] E. Soignard, P.F. McMillan, C. Hejny, K. Leinenweber, Pressure-induced transformations in α - and β -Ge₃N₄: in situ studies by synchrotron X-ray diffraction, *J. Solid State Chem.* 177 (2004) 299–311, <https://doi.org/10.1016/j.jssc.2003.08.021>.
- [26] J.C. Jie, C.M. Zou, H.W. Wang, B. Li, Z.J. Wei, Enhancement of mechanical properties of Al-Mg alloy with a high Mg content solidified under high pressures, *Scripta Mater.* 64 (2011) 588–591, <https://doi.org/10.1016/j.scriptamat.2010.11.049>.
- [27] X.H. Wang, Z. Ran, Z.J. Wei, C.M. Zou, H.W. Wang, J. Gouchi, Y. Uwatoko, The formation of bulk β -Al₃Ni phase in eutectic Al-5.69wt%Ni alloy solidified under high pressure, *J. Alloy. Compd.* 742 (2018) 670–675, <https://doi.org/10.1016/j.jallcom.2018.01.272>.
- [28] K. Zhao, S. Wu, S.Y. Jiang, H.Z. Zhang, K.K. Song, T. Wang, H. Xing, L.M. Zhang, K. F. Li, L. Yang, X.L. Wang, L. Wang, Microstructural refinement and anomalous eutectic structure induced by containerless solidification for high-entropy Fe-Co-Ni-Si-B alloys, *Intermetallics* 122 (2020) 106812, <https://doi.org/10.1016/j.intermet.2020.106812>.
- [29] X.M. Liu, Z.D. Kou, R. T Qu, W.D. Song, Y.J. Gu, C.S. Zhou, Q.W. Gao, J.Y. Zhang, C.D. Cao, K.K. Song, V. Zadorozhnyy, Z.Q. Zhang, J. Eckert, Accelerating matrix/boundary precipitations to explore high-strength and high-ductile Co₃₄Cr₃₂Ni₂₇Al_{3.5}Ti_{3.5} multicomponent alloys through hot extrusion and annealing, *J. Mater. Sci. Technol.* 143 (2023) 62–83, <https://doi.org/10.1016/j.jmst.2022.08.052>.
- [30] T.T. Shun, L.Y. Chang, M.H. Shiu, Age-hardening of the CoCrFeNiMo_{0.85} high-entropy alloy, *Mater. Char.* 81 (2013) 92–96, <https://doi.org/10.1016/j.matchar.2013.04.012>.
- [31] O. Conejero, M. Palacios, S. Rivera, Premature corrosion failure of a 316L stainless steel plate due to the presence of sigma phase, *Eng. Fail. Anal.* 16 (2009) 699–704, <https://doi.org/10.1016/j.engfailanal.2008.06.022>.
- [32] A. Takeuchi, A. Inoue, Classification of bulk metallic glasses by atomic size difference, heat of mixing and period of constituent elements and its application to characterization of the main alloying element, *Mater. Trans.* 46 (2005) 2817–2829, <https://doi.org/10.2320/matertrans.46.2817>.
- [33] Y. Zhang, Y.J. Zhou, J.P. Lin, G.L. Chen, P.K. Liaw, Solid-Solut-ion phase formation rules for multi-component alloys, *Adv. Eng. Mater.* 10 (2008) 534–538, <https://doi.org/10.1002/adem.200700240>.
- [34] X. Yang, Y. Zhang, Prediction of high-entropy stabilized solid-solution in multi-component alloys, *Mater. Chem. Phys.* 132 (2012) 233–238, <https://doi.org/10.1016/j.matchemphys.2011.11.021>.
- [35] S. Guo, C. Ng, J. Lu, C.T. Liu, Effect of valence electron concentration on stability of fcc or bcc phase in high entropy alloys, *J. Appl. Phys.* 109 (2011) 103505, <https://doi.org/10.1063/1.3587228>.
- [36] Y. Zhang, Z.P. Lu, S.G. Ma, P.K. Liaw, Z. Tang, Y.Q. Cheng, M.C. Gao, Guidelines in predicting phase formation of high-entropy alloys, *MRS Commun* 4 (2014) 57–62, <https://doi.org/10.1557/mrc.2014.11>.
- [37] R.R. Chen, G. Qina, H.T. Zheng, L. Wang, Y.Q. Su, Y.L. Chiu, H.S. Ding, J.J. Guo, H. Z. Fu, Composition design of high entropy alloys using the valence electron concentration to balance strength and ductility, *Acta Mater.* 144 (2018) 129–137, <https://doi.org/10.1016/j.actamat.2017.10.058>.
- [38] G. Cheng, K.S. Choi, X. Hu, X. Sun, Determining individual phase properties in a multi-phase Q&P steel using multi-scale indentation tests, *Mater. Sci. Eng.* 652 (2016) 384–395, <https://doi.org/10.1016/j.msea.2015.11.072>.
- [39] Y.X. Ye, B. Ouyang, C.Z. Liu, G.J. Duscher, T.G. Nieh, Effect of interstitial oxygen and nitrogen on incipient plasticity of Nb₂TiZrHf high-entropy alloys, *Acta Mater.* 199 (2020) 413–424, <https://doi.org/10.1016/j.actamat.2020.08.065>.
- [40] B.J. Wang, Q.Q. Wang, N. Lu, X.B. Liang, B.L. Shen, Enhanced high-temperature strength of HfNbTaTiZrV refractory high-entropy alloy via Al₂O₃ reinforcement, *J. Mater. Sci. Technol.* 123 (2021) 191–200, <https://doi.org/10.1016/j.jmst.2022.01.025>.
- [41] J.A. Smeltzer, B.C. Hornbuckle, A.K. Giri, K.A. Darling, M.P. Harmer, H.M. Chan, C. J. Marvel, Nitrogen-induced hardening of refractory high entropy alloys containing laminar ordered phases, *Acta Mater.* 211 (2021) 116884, <https://doi.org/10.1103/10.1016/j.actamat.2021.116884>.